

# A scheme for the determination of the magnetic field in the KATRIN main spectrometer

---

**A. Osipowicz<sup>a,\*</sup>, U. Rausch<sup>a</sup>, A. Unru<sup>a</sup>, B. Zipfel<sup>b</sup>**

<sup>a</sup> *Department of Electrical Engineering and Information Technology, University of Applied Sciences, Marquardstr. 35, Fulda, Germany*

<sup>b</sup> *HF-Dept., GSI Helmholtzzentrum für Schwerionenforschung GmbH, Planckstrasse 1, D-Darmstadt, Germany*

*E-mail:* Alexander.Osipowicz@et.hs-fulda.de

**ABSTRACT:** To determine the magnetic field distribution in the KATRIN main-spectrometer with magnetic field sensors that are placed outside the main-spectrometer vessel one can utilize the absence of magnetic rotation in main-spectrometer volume. There a scalar magnetic potential  $V(\vec{x})$  can be defined that fulfills the Laplace equation. Large numbers of magnetic field values on an outer surface of the main-spectrometer can be sampled by moving and fixed magnetic field sensors. These surface samples are used as boundary values in the relaxation of the Laplace equation for  $V(\vec{x})$  and the magnetic field components in the volume. In a simulation involving the KATRIN reference solenoid chain, a global magnetic field and an external perturbing solenoid it is shown that with this method the original field can be reconstructed within 2 %.

**KEYWORDS:** Spectrometers; Detector alignment and calibration methods (lasers, sources, particlebeams); Detector control systems (detector and experiment monitoring and slow-control systems, architecture, hardware, algorithms, databases).

---

\*Corresponding author.

---

## Contents

1. The KATRIN setup	1
2. Volume and surface considerations	2
3. Simulation	3
4. Simulation results	5
5. Summary and Outlook	8

---

### 1. The KATRIN setup

The KARlsruhe TRItium Neutrino experiment [1] (see Fig.1) is set up at the Karlsruher Institute of Technology (KIT), Germany. It is designed to measure the mass of the electron anti neutrino in a direct and model-independent way with a sensitivity of  $m_\nu = 0.2 \text{ eV}/c^2$  (90% confidence level) from tritium  $\beta$  decay[1]. KATRIN uses a magnetic transport field that connects the source and detector in combination with integrating electrostatic energy filters (MAC-E-spectrometers). Conceptual essentials of the MAC-E spectrometer[2, 3] are the magnetic field gradients in pre - and main-spectrometer that adiabatically convert cyclotron energy  $E_{cyc}$  into energy  $E_p$  parallel to the magnetic field lines and vice versa.

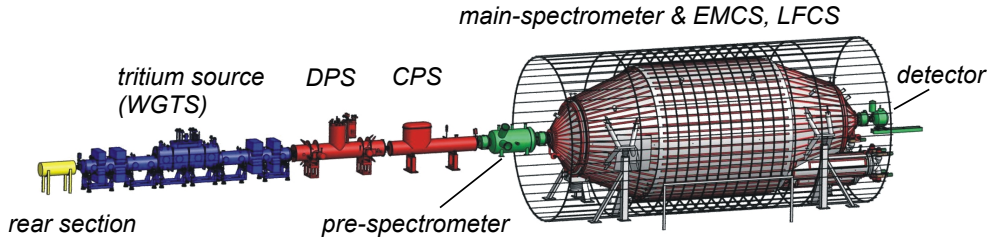


**Figure 1.** Schematic view of the KATRIN experiment (total length 70 m) consisting of calibration and monitor rear system, with the windowless gaseous  $T_2$ -source (WGTS), differential pumping (DPS) and cryo-trapping section (SPS), the small pre-spectrometer and the large main spectrometer with the large magnetic coil systems to compensate the earth magnetic field (EMCS) and to shape the magnetic transport flux (LFCS) and lastly the segmented PIN-diode detector.

At the center of the main-spectrometer (MS) in the minimal magnetic field  $B_A \approx 3 - 6 \mu\text{T}$ , a retarding electric field allows an integral energy analysis of  $E_p$ . The magnetic field in the analyzing

volume defines the magnetic resolution, i.e. the amount of residual cyclotron energy  $E_{cyc}$  that can not be analyzed and thus strongly influences the resolution function. Error analysis [4] of the influence of uncertainty of the magnetic field in the analyzing plane on the uncertainty of the neutrino mass square  $\Delta m_\nu^2$  leads to a relative accuracy of the magnetic field of  $\frac{\Delta B}{B} < 2.4\%$ . In addition, the alignment of magnetic field lines plays a crucial role in the production of secondary electrons and electronic background either through penning traps or inner wall contact.

Large coil systems [5] are arranged around the MS for a) global magnetic field compensation, e.g. earth magnetic field (EMCS) and b) fine tuning of the magnetic transport flux with a set of large circular low field coils (LFCS) mounted coaxially with the MS (see Fig.1). However, possible influences of residual external dipoles, magnetization in the MS environment by the high field solenoids and/or EMCS, LFCS and the correct orientation of the spectrometer solenoids have to be controlled. Due to the extreme MS vacuum conditions the installation of magnetic sensors inside the MS is not possible.

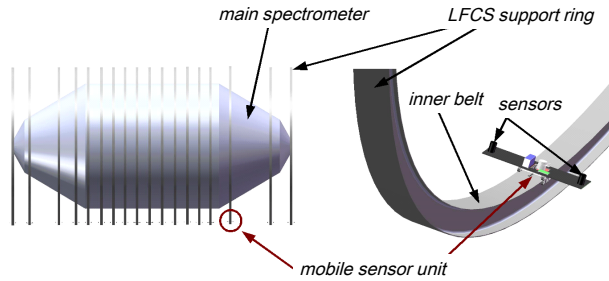


**Figure 2.** View of the main spectrometer tank with the LFCS ring system. Right: The mobile sensor unit with 2 sensors on the inner belt of a LFCS support ring.

We therefore propose to determine the magnetic field *inside* the main spectrometer by taking magnetic field samples at an outer surface of the main spectrometer. The sensor network will involve fixed position magnetic sensors and mobile magnetic field sensors [6, 7, 8] which move along the inner belts of the LFCS support structure (see Fig.2), close to the outer MS surface but well inside the current lines of the EMCS and LFCS. The magnetic field samples serve as boundary values for the relaxation of the Laplace equation of the scalar magnetic potential  $V(\vec{x})$  at the interior of the KATRIN main spectrometer.

## 2. Volume and surface considerations

For a volume  $G$  with surface area  $\Gamma$  Amperes equation

$$\vec{\nabla} \times \vec{B} = \mu_0 \cdot \left( \vec{J} + \frac{\epsilon_0 \cdot \partial \vec{E}}{\partial t} \right) \quad (2.1)$$

can be simplified to the rotationally free case if the current density  $\vec{J}$  is vanishing ( $J = 0$ ) and the electric field  $\vec{E}$  is constant ( $\partial \vec{E} / \partial t = 0$ ).

$$\vec{\nabla} \times \vec{B} = 0 \quad (2.2)$$

For the KATRIN MS the relevant surface  $\Gamma$  (see Fig.3) has to be outside the outer MS surface and inside the current leading elements (LFCS, EMCS, spectrometer solenoids). As the analyzing potential distribution  $U(x,y,z)$  inside the MS volume is constant during KATRIN runtime intervals (and magnetic field sampling time intervals) the electrical fields produced are time independent. Therefore eq. (2.2) can assumed to be valid for the KATRIN MS interior.

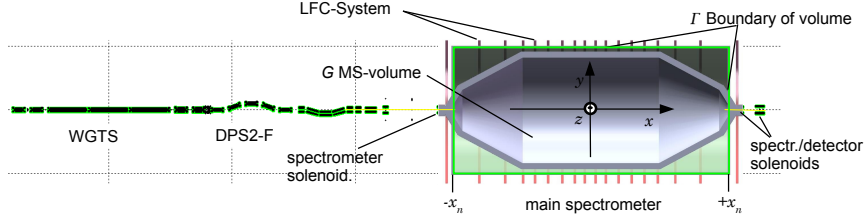


**Figure 3.** View of the KATRIN main reference solenoid chain and the main spectrometer area. The cylindrical volume  $G$  enclosed by the boundary  $\Gamma$ . The origin of the coordinate system is located at the geometrical center of the MS and the symmetry point of the LFCS. To ensure that all current leading elements are outside the boundary  $\Gamma$  in  $y$ - and  $z$ - direction the allowed radius  $R_G$  to  $G$  is  $5600 \text{ mm} < R_G < 6155 \text{ mm}$ . The extreme  $x$ - values are  $-11600 \text{ mm} = -x_n < x < +x_n = 11600 \text{ mm}$ .

Vector analysis [10] states for a scalar function  $V(\vec{x})$  that:  $\vec{\nabla} \times \vec{\nabla} \cdot V(\vec{x}) = 0$  and one can identify  $V(\vec{x})$  with the magnetic scalar potential.

$$\vec{B} = \vec{\nabla} \cdot V(\vec{x})$$

Utilizing Gauss's law for magnetism  $\vec{\nabla} \cdot \vec{B} = 0$  we can write down the *Laplace-equation* (LPE) for  $V(\vec{x})$

$$\nabla^2 V(x,y,z) = 0 \quad (2.3)$$

The finite difference method (FDM) [11] is chosen to solve the above equation on a 3 dimensional rectangular grid, because of its well known numerical stability and the manageable coding effort. In the simulation the magnetic field components at a the boundary representing the normal derivatives  $\partial V / \partial x = B_x$ ;  $\partial V / \partial y = B_y$ ;  $\partial V / \partial z = B_z$  at  $\Gamma$  can be exported and used in the FD-relaxation as a *von Neumann boundary* values.

### 3. Simulation

The usability of the numerical approach is demonstrated in a simulation based on magnetic field values provided by the simulation package **PartOpt** [9]. The definition of a magnetic scenario (Fig. 4) at the KATRIN main spectrometer includes: a) the energized KATRIN reference solenoid chain, b) the energized LFCS as listed in [13], c) a magnetic field over  $G$  with  $B_x = 210 \text{ mG}$ ,  $B_y = 35 \text{ mG}$ ,  $B_z = 0$ , d) a small disturbing magnetic dipole with central induction  $B_c = 600 \text{ G}$  adjacent to the main spectrometer.

The field values  $B_x, B_y, B_z$  along the cylindrical surface of volume  $G$  with radius  $R_G = 6 \text{ m}$  between  $x_{min} = -7.03 \text{ m} < x < x_{max} = 6.83 \text{ m}$  to cover the cylindrical part of the MS are exported in ASCII format. The spacing of the samples in  $x$ -direction is  $0.45 \text{ m}$  in agreement with the real  $x$ -spacing of the sensor positions. In azimuthal direction a  $3^\circ$  spacing was chosen to get  $120 \times 2$

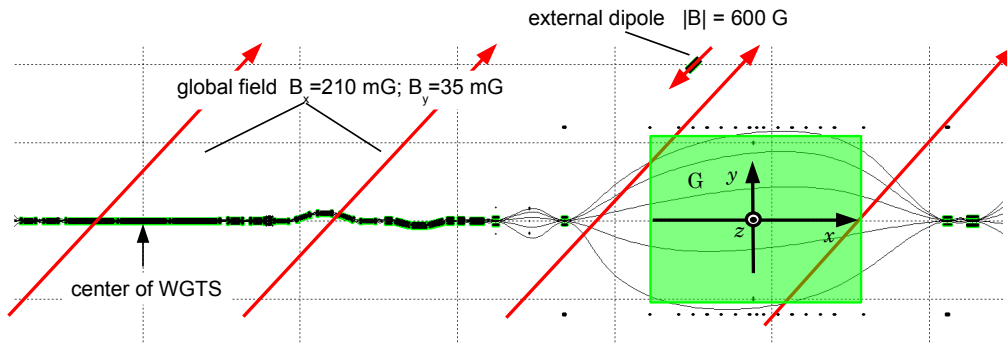


**Figure 4. PartOpt** view of the Simulation scenario. In volume  $G$  the effective magnetic field is composed of the KATRIN solenoid field, LFCS, an external global field and disturbing external dipole. The perturbed magnetic field lines magnetic field lines have been tracked starting from the center of the WGTS. The extreme field lines indicate the boundary of the  $191 \text{ T cm}^2$  nominal magnetic transport flux connecting source and detector.

samples (because 2 sensors are on board) in 15 minutes, the time for one revolution. To simulate sensor error the exported values are randomized according to a Gaussian distribution with a 2% relative uncertainty. This value was chosen as an upper limit according to the sensor types used in [6]. Due to the cylindrical geometry the surface samples points usually do not coincide with surface mesh points (cut surfaces problem). Therefore the magnetic samples are interpolated to produce values at the regular surface mesh points. The relaxation is performed via a basic 7 point stencil. The resulting values for the scalar potential and the values for the magnetic field components are generated by deriving  $V(\vec{x})$  numerically.

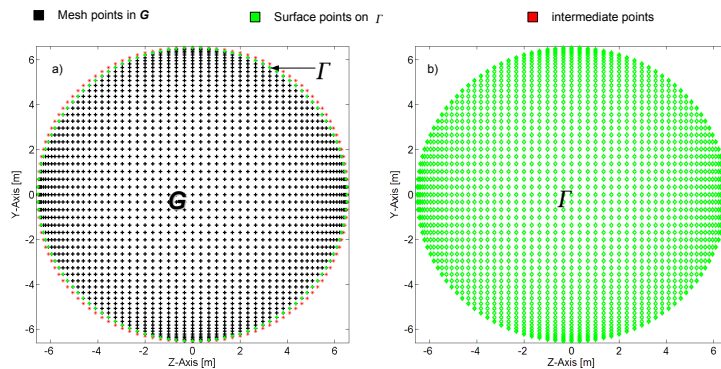


**Figure 5.** View of the mesh point structure. Left:  $G$  in an interval in  $z$ ,  $-x_n < z < x_n$ , Right: on the surface  $\Gamma$ , at  $z = -x_n, x_n$

The relaxation code is written in C. Typically 1400 iterations in 5 minutes on a standard PC are performed to meet the terminating condition that the difference for  $V(0,0,0)$ , the magnetic potential at the origin, between successive iterations is  $< 0.0002$ .

#### 4. Simulation results

The results of the simulation is displayed as magnetic field components in geometric planes with given coordinates within the main spectrometer. Figs.: 6,8,10 show the original **PartOpt** magnetic  $B_{org}$  and the reconstructed magnetic field  $B_{rec}$  components for a randomly chosen  $x,y$  plane at  $z = 2.4994$  m. The relative differences  $\Delta B$  are displayed in Fig.: 7,9,11,.

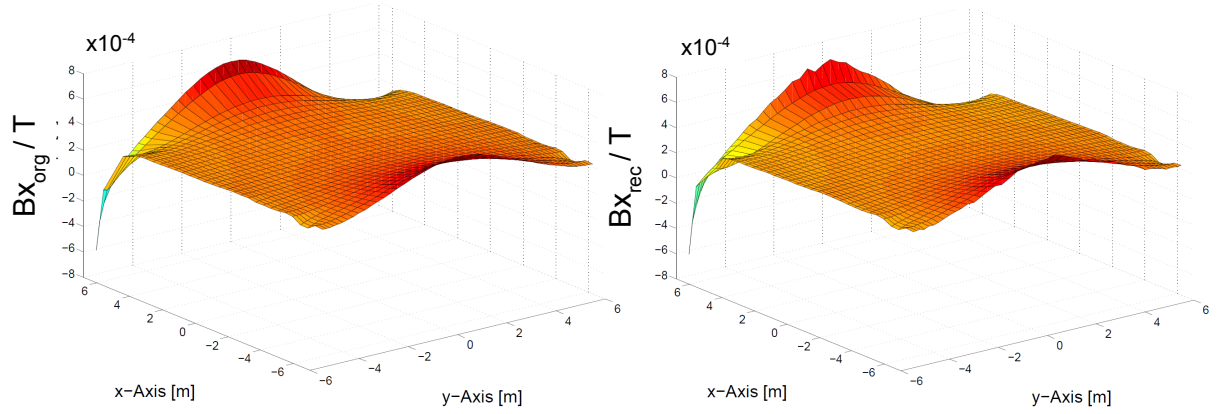


**Figure 6.** Left: The original magnetic field component  $B_{x_{org}}$  in a in a  $x,y$  plane at  $z = 2.4994$  m. Right: The reconstructed magnetic field values  $B_{x_{rec}}$  in the same plane.

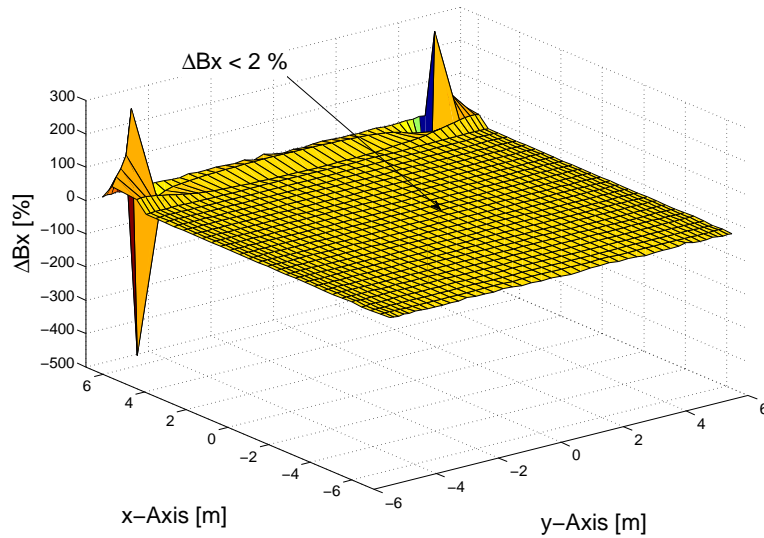


**Figure 7.** Relative difference between the original  $B_{x_{org}}$  and reconstructed  $B_{x_{rec}}$  magnetic field component  $\Delta B_x = (B_{x_{org}} - B_{x_{rec}})/B_{x_{org}}$  in a  $x,y$  plane with  $z = 2.4994$  m. The sharp peaks at  $x \approx 6$  arise numerically from a division by zero as  $B_{x_{org}} \approx 0$  in the vicinity of the negatively charged LFCS coil towards the detector side as given in [13]. Elsewhere the difference is less than 2%.

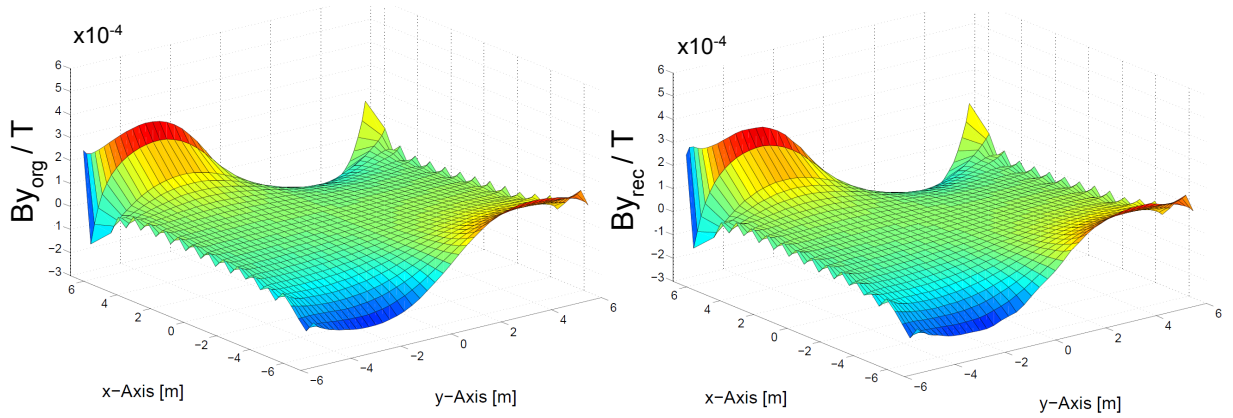


**Figure 8.** Left: The original magnetic field component  $B_{y_{org}}$  in a in a  $x, y$  plane at  $z = 2.4994$  m. Right: The reconstructed magnetic field values  $B_{y_{rec}}$  in the same plane. The sawtooth structure at the extreme  $y$ -values are due to the close proximity of the energized LFCS Coils.

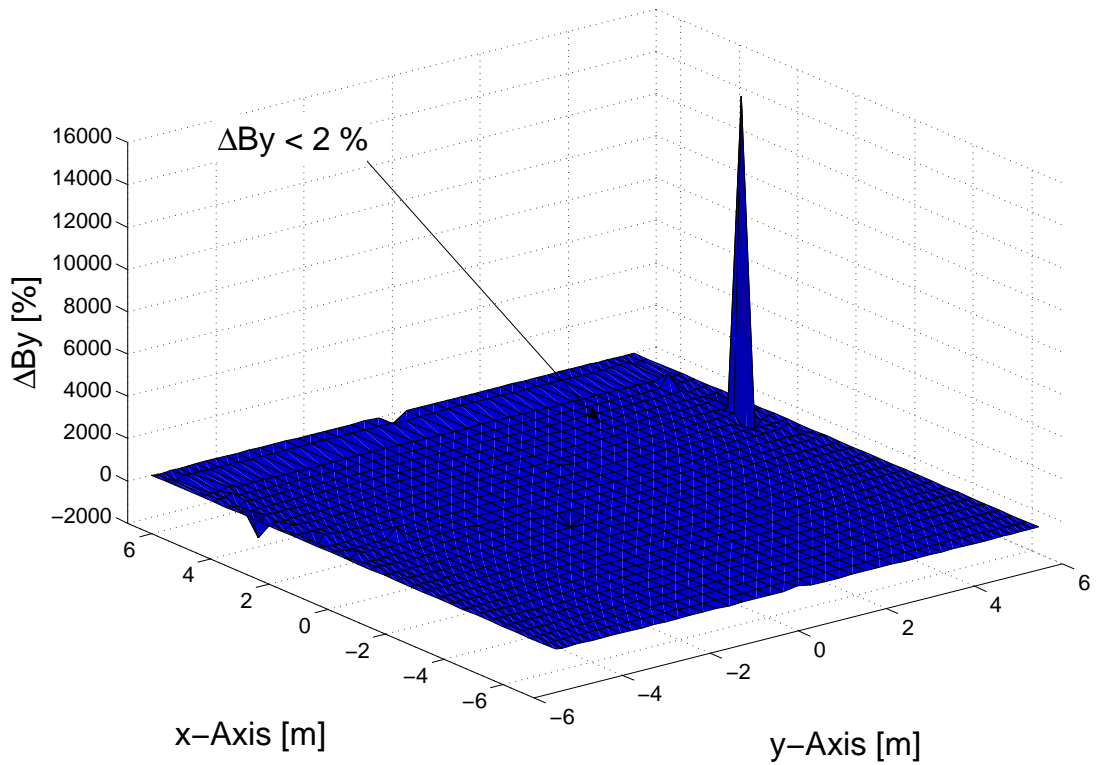


**Figure 9.** Relative difference between the original  $B_{y_{org}}$  and reconstructed  $B_{y_{rec}}$  magnetic field component  $\Delta B_y = (B_{y_{org}} - B_{y_{rec}}) / B_{y_{org}}$  in a  $x, y$  plane with  $z = 2.4994$  m. The sharp peaks arise numerically from a division by zero as  $B_{y_{org}} \approx 0$ .

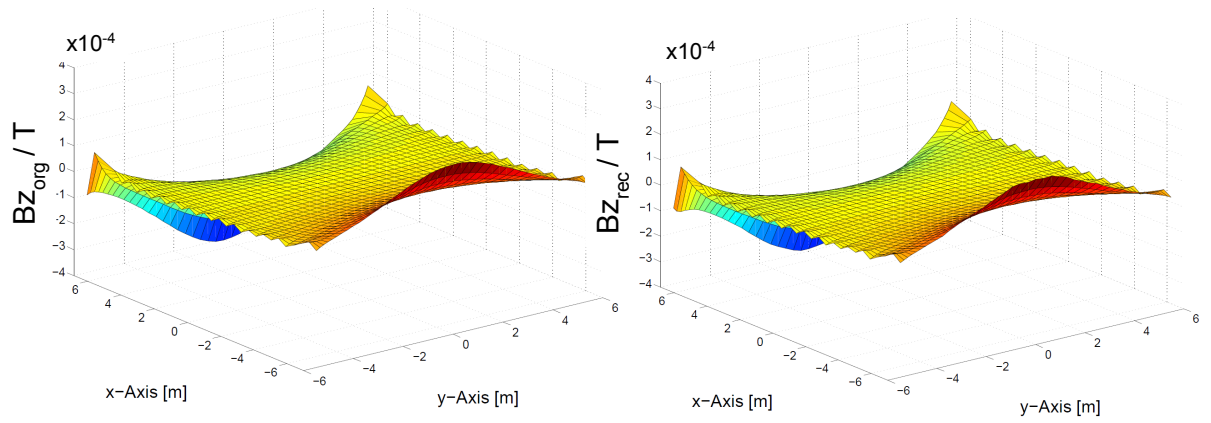


**Figure 10.** Left: The original magnetic field component  $B_{z_{org}}$  in a  $x, y$  plane at  $z = 2.4994$  m. Right: The reconstructed magnetic field values  $B_{z_{rec}}$  in the same plane. The sawtooth structure at the extreme  $y$ -values are due to the close proximity of the energized LFCS Coils.

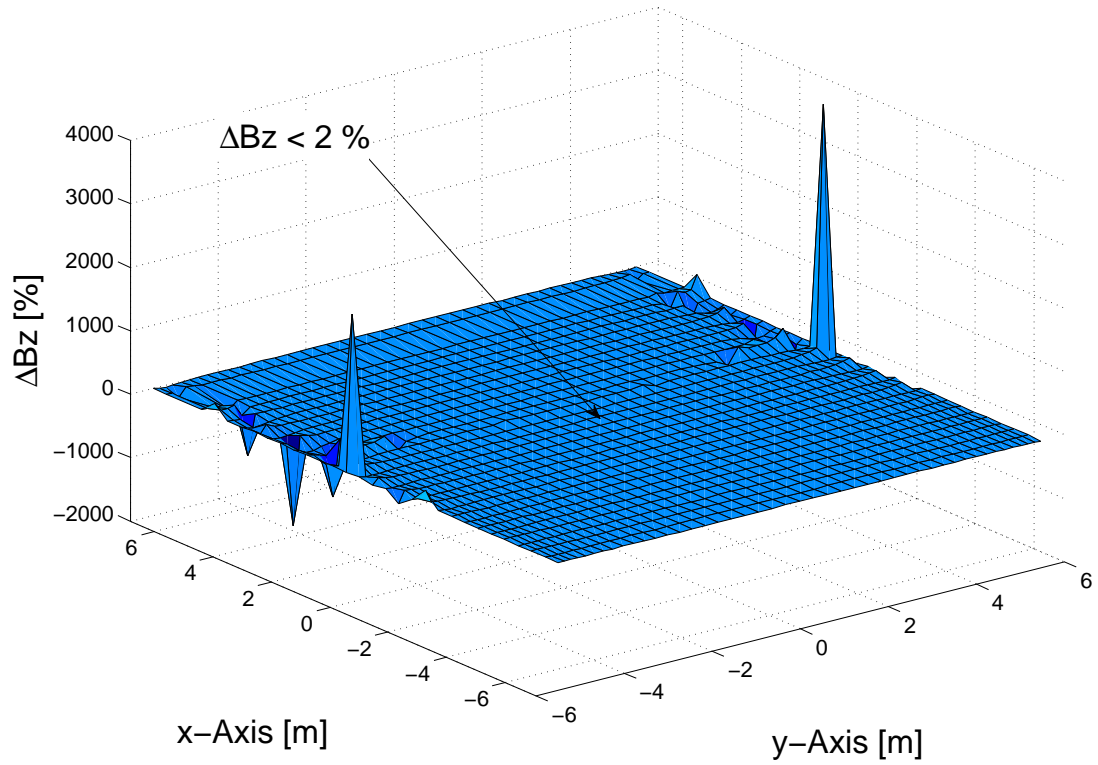


**Figure 11.** Relative difference between the original  $B_{z_{org}}$  and reconstructed  $B_{z_{rec}}$  magnetic field component  $\Delta B_z = (B_{z_{org}} - B_{z_{rec}}) / B_{z_{org}}$  in a  $x, y$  plane with  $z = 2,4994$  m. The sharp peaks at extreme  $y$ -values arise numerically from a division by zero as  $B_{z_{org}} \approx 0$ .

Results with similar precision can be found in all areas of the inner volume. Fig. 12 shows the relative difference  $\Delta B_x$  for a  $y, z$ -plane at  $x = 2.475$  m.

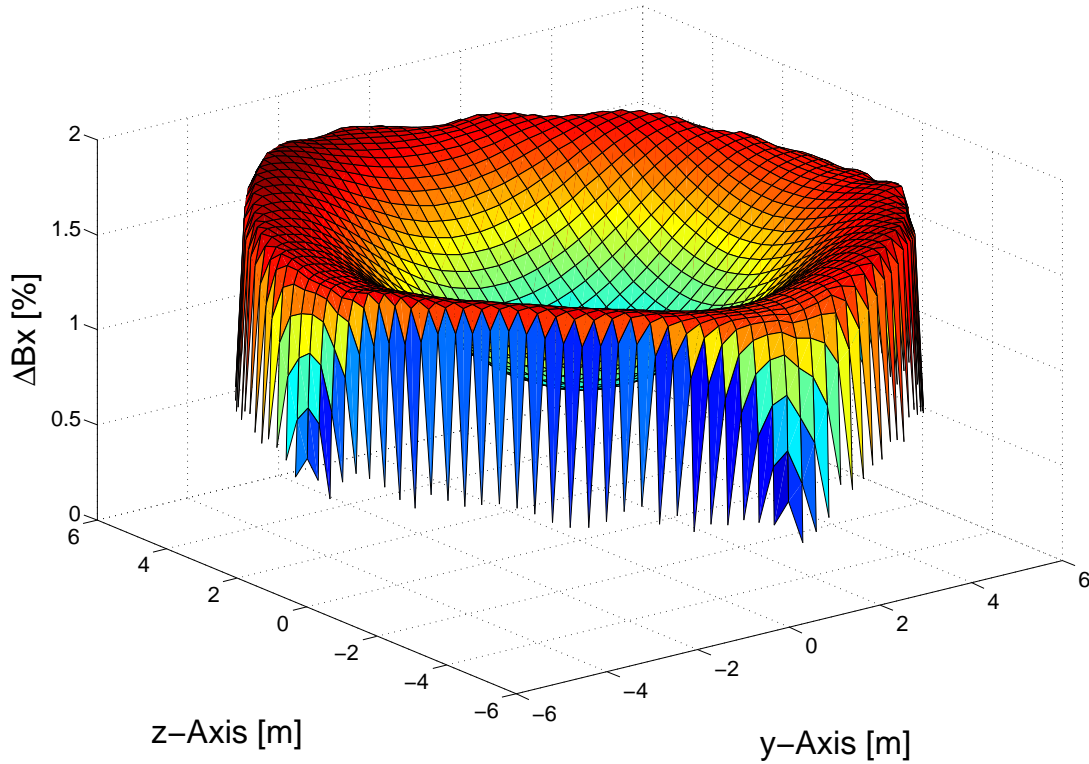


**Figure 12.** Relative difference between the original  $B_{x_{org}}$  and reconstructed  $B_{x_{rec}}$  magnetic field component  $\Delta B_x = (B_{x_{org}} - B_{x_{rec}})/B_{x_{org}}$  in a  $z, y$  plane with  $x = 2.475$  m. The sawtooth structure at the fringes is due to the vanishing  $B - x$ -component at large radii.

## 5. Summary and Outlook

In a simulation it is shown that with a large number of magnetic field samples taken close to the KATRIN main-spectrometer surface and inside the current leading elements of the LFSC -, EMCS system and spectrometer solenoids it is possible to determine the magnetic field profile inside the spectrometer at least within a 2% precision. With better numerical techniques (e.g. stencils involving more meshpoints, interpolation routines with more supporting points) and longer computer relaxation times an increase in precision is possible. Also the number and distribution of the sampling positions on the surface can in the case of the mobile sensor units be varied to achieve better results.

As the front face (at  $-x_n$ ) and the end face (at  $+x_n$ ) of the cylindrical volume still intersect the KATRIN MS volume no samples can be taken there. However, the magnetic field of these surfaces is predominantly given by the spectrometer solenoids which can be modeled numerically to produce calculated field values. These models can be controlled by fixed position magnetic field sensors close to the relevant surfaces.

Unlike in a simulation, where the magnetic field components are per se given according to the chosen coordinate system, the magnetic field sensors in KATRIN environment have to be aligned according to the KATRIN global coordinate system. In the case of moving sensor units moving on the inner rails of the LFCS structure as proposed in [6] this requires information about position and inclination along the track.

## AKNOWLEDGMENTS

The authors wish to express gratitude to the group for Experimental Techniques of the Institute for Nuclear Physics (IK) at KIT for highly efficient and competent support. Furthermore, we wish to thank Prof. Dr. E. W. Otten, Mainz University and Prof. Dr. Ch. Weinheimer, Münster University for helpful discussions and support. In addition, we like to thank the University of Applied Sciences, Fulda and the Fachbereich Elektrotechnik und Informationstechnik, for the enduring support for this work.

This work has been funded by the German Ministry for Education and Research under the Project codes 05A11REA, 05A08RE1.

## References

- [1] KATRIN collaboration, *KATRIN design report 2004*, technical report, Forschungszentrum Karlsruhe, <http://www-ik.fzk.de/>, Karlsruhe Germany (2004).
- [2] A. Picard et al., *A solenoid retarding spectrometer with high resolution and transmission for keV electrons*, Nucl. Instrum. Meth. B 63 (1992) 345.
- [3] V.M. Lobashev and P.E. Spivac, *A method for measuring the anti-electron-neutrino rest mass*, Nucl. Instrum. Meth. A 240 (1985) 305.
- [4] K. Valerius, *Elektromagnetisches Design für das Hauptspektrometer des KATRIN Experiments*, Diploma-Thesis, Universität Bonn, 2004
- [5] A. Osipowicz and F. Glück, *Air coil design at the main spectrometer*, KATRIN internal document, <http://fuzzy.fzk.de/bscw/bscw.cgi/d443733/95-TRP-4440-D1-F.Glueck-A.Osipowicz.ppt>.
- [6] A. Osipowicz, W. Seller, J. Letnev, P. Marte, A. Müller, A. Spengler and A. Unru *A mobile magnetic sensor unit for the KATRIN main spectrometer*, 2012 JINST 7 T06002; arXiv:1207.3926
- [7] A. Unru, *Elektrische und mechanische Konzipierung und prototypische Realisierung einer mobilen Sensoreinheit* (in German), Diploma-Thesis, Univ. of Appl. Sciences, Fulda, Germany, July 2009.
- [8] J. Letnev, *Systemintegration des Magnetfeldsensornetzes* (in German), Master-Thesis, Univ. of Appl. Sciences, Fulda, Germany May 2011.
- [9] *The PartOpt project webpage*, <http://www.PartOpt.net/>
- [10] T. M. Apostol, *Mathematical Analysis*, Addison-Wesley, 4th ed. 1971, p. 312, *Library of Congress Catalog Card No.* 57-8707
- [11] H. R. Schwarz, N. Koeckler, *Numerische Mathematik*, 6.Auflage B.G. Teubner Verlag / GWE Fachverlage GmbH, Wiesbaden

- [12] S. Flachs, A. Osipowicz, A. Unru, *Design Document, A wireless magnetic sensor grid for the KATRIN mainspectrometer*, KATRIN internal document <https://fuzzy.fzk.de/bscw/bscw.cgi/d698744/>
- [13] Fernec Glueck et al., *New pinch, detector and axisymmetric air coil design*, KATRIN internal document, *95-TRP-4341-D1-FGlueck.ppt*